Macromolecules
ARTICLE

Macromolecules **2009**, *42*, 5189–5195 **5189**
DOI: 10.1021/ma900249z

Crystallinity in Ethene−1-Hexene Copolymers Determined by ^{1}H and ^{13}C NMR. A Comparative Study

Lili Zhang,[†] Eddy W. Hansen,*[,†] Irene Helland,[§,⊥] Einar Hinrichsen,[‡] Åge Larsen,[‡] and Jaan Roots[†]

[†]*University of Oslo, Department of Chemistry, UiO, P.O. Box 1033 Blindern, N-0315 Oslo, Norway,* [‡]*SINTEF Materials and Chemistry, P.O.Box 124 Blindern, N-0314 Oslo, Norway, and* [§]*Borealis AS, N-3960 Stathelle, Norway.* [⊥]*Present address: Norner Innovation AS, Asdalstrand 291, N-3960 Stathelle, Norway*

Received February 4, 2009; Revised Manuscript Received June 8, 2009

ABSTRACT: The ^{13}C DD-MAS spectra of six ethene/1-hexene (E/H) copolymers were fitted simultaneously to a sum of four pseudo Voigt functions in which two were assigned to the all-*trans* crystalline region. These two peaks possessed the same chemical shift but differed in both line width and line shape. Regarding the amorphous region, it was found to be represented by a sum of a Lorenzian function and a Gaussian function possessing different chemical shifts. The latter simply reflects the asymmetry of the spatial distribution of trans−gauche conformations. The crystallinity of the samples, as determined by DSC, was found to be in excellent agreement with the crystallinity determined from ^{13}C DD-MAS spectra. Moreover, the crystalline part of the ^{1}H-FID (acquired at 0.5 and 4.7 T) was fitted by using a Pake function and Abragamian function, respectively. The latter was found to give a crystallinity in quantitative agreement with the ^{13}C DD-MAS and DSC. In contrast, the replacement of the Abragamian function with a Pake function (to represent the crystalline part of the FID) resulted often in unstable and poor model fits with rather unreliable estimate of the crystallinity. The inherent problem related to the necessary blanking of the receiver during the initial part of the FID (dead-time) is discussed.

Introduction

From a phenomenological point of view, a semicrystalline polymer can be considered to be crystallites embedded in a noncrystalline (amorphous) matrix in which the mass-fraction or volume-fraction of crystallites define the crystallinity. Any experimental method sensitive to the difference in physical properties between the two domains constitutes a potential technique to probe crystallinity. For many years a great deal of effort has been invested to accurately determine crystallinity of semicrystalline polymers, since it correlates with the mechanical properties of the polymer.[1,2] Consequently, crystallinity has become an important term within all branches of polymer activity.

The simplest experimental technique to probe crystallinity is to measure the density.[3] However, for decades a large number of other experimental methods, like differential scanning calorimetry (DSC), X-ray diffraction (XRD) and various spectroscopic techniques (NMR, IR, Raman) have been adopted to explore the various aspects of crystallinity.[4−7] In particular, DSC seems to have been implemented in the industry as a routine technique for measuring crystallinity.

Various solid-state NMR techniques have been frequently applied[8−11] to derive the crystallinity of semicrystalline polymers during the past decade. These experimental techniques are sensitive to differences in molecular dynamics and/or molecular structures. In particular, proton free-induction decay (^{1}H-FID) analysis has become increasingly popular as it combines the advantages of being rather sensitive, robust, fast and nearly independent of the magnetic field strength. Moreover, the crystallinity derived from ^{1}H-FID NMR is nearly magnetic field independent, which allows the adoption of less costly low-field NMR spectrometers.

*Corresponding author. Fax: +47 22855441. E-mail: eddywh@kjemi.uio.no.

However, the inherent noise in the initial part of the FID (as caused by rf-pulse breakthrough) calls for a time delay in the start of the acquisition and results in crystallinites that are smaller than the "true" crystallinity.[12−15] The ringing effects in the beginning of the FID are possible to eliminate by using a composite pulse with suitable phase cycling.[16] The most elegant and simplified approach to overcome the dilemma of rf-breakthrough is, nevertheless, to implement specialized equipment to reduce the dead time to the order of 1−2 μs.[17−19]

Litvinov et al.[20] adopted a solid-echo technique to refocus the dipolar interaction and claimed that reliable crystallinity could be obtained by a so-called "back-extrapolation" technique during data processing. However, this necessitates an increasing number of experiments using different echo delays and results in an overall increase in experimental time. Zhang et al.[21] proposed a windowless solid echo which reduced the effect of inhomogeneous rf field and long delay time in conventional solid echo.

Saalwächter and co-workers[11] have recently proposed a mixed magic-sandwich echo (MSE) technique[22,23] aiming at refocusing the initial part of the FID which, unfortunately, did not work out for polyethylene (PE). Work is in progress to understand this dilemma.

It has been recognized that the use of solid-state NMR provides crystallinity from various NMR observables such as line-width, chemical shift and ^{13}C spin−lattice relaxation time T_1.[24−26] Although ^{13}C signal arising from an undisturbed Boltzmann equilibrium population gives rigorous and quantitative relative signal intensities, the low natural abundance and the long $T_1{}^{C}$ make conventional single pulse carbon detection without cross-polarization (CP) rather time-consuming. The most frequent method to determine crystallinity by solid-state ^{13}C NMR involves cross-polarization under magical angle spinning (MAS).[8−10]

Interestingly, Young et al.[27] obtained the crystallinity of PE from a static (no MAS) ^{13}C NMR spectrum involving CP and

Published on Web 06/25/2009

based on chemical shift anisotropy (chemical shift tensor) analysis. Although this method is experimentally faster than a conventional single-pulse carbon experiment, we consider—at present—the practical use of this approach to be somewhat questionable.

A novel NMR experimental approach to determine crystallinity was presented recently by Hansen and co-workers and involves a combined use of proton spin-diffusion (SD) and ^{13}C CP-MAS.[28] To what extent this technique can be used as a routine analysis in determining crystallinity needs further exploration.

One question which needs to be addressed is to what extent different NMR techniques give consistent crystallinities. Only a few[8,29] reports exist in the open literature which addresses this topic systematically. For instance Asano et al.[8] found that the crystallinity of poly(ε-L-lysine), as derived from ^1H NMR and ^{13}C NMR, deviated significantly. Similar studies on PE were not found despite a thorough search in the literature. In this work, NMR crystallinity of linear low density polyethylene (LLDPE) samples (crystallinity between 45 and 60%) obtained from ^1H-FID and ^{13}C DD-MAS (one pulse excitation with high power decoupling) NMR is discussed and compared with crystallinity obtained by DSC.

Experimental Section

Samples. Polyethylene (PE) copolymers with different amount (mole-fraction, f_{hexene}, or mass-fraction, w_{hexene}) of comonomer (1-hexene) were synthezised by Borealis AS, Norway, using a single-site (metallocene) catalyst and provided in powder form. The samples were stabilized with Irganox B220 (1000 ppm), and after careful homogenization pressed into plates 50 mm × 50 mm × 2 mm (first kept at 220 °C for 3 min, then cooled at 40 °C/min to below 80 °C, and subsequently to 20 °C at a lower cooling rate). Characteristic data for the copolymers are summarized in Table 1.

DSC Measurements. The thermal analysis was done on a computerized Perkin-Elmer model Pyris 1, using Pyris software. Sample masses of 1.5−2 mg were used in this study. During the measurement, dried N_2 gas was purged at a constant flow rate. Heating rates of 10 °C were used for the melting endotherms (in the range 20−180 °C). All endotherms were baseline corrected using empty aluminum pans. Temperature and enthalpy calibrations were performed with indium and zinc at the same heating rate. Enthalpy-based mass crystallinities, w(DSC), were calculated according to the procedure described by Mathot and Pijpers,[31] and using the ATHAS database.[32] The results for the samples as cut from the pressed plates (first heating) are given in Table 1.

NMR Measurement. Fully relaxed proton decoupled ^{13}C-DD-MAS NMR spectra were carried out at room temperature (23 °C) on a Bruker DSX-300 spectrometer operating at 75.47 MHz. The PE samples were cut and packed into a magic angle spinning (MAS) rotor, having a diameter of 4 mm. The MAS rate was set to 5 kHz, and the proton 90° pulse width was set to 2.6 μs. Carbon chemical shifts were referenced to the chemical shift of the carbonyl carbon (δ = 176.03 ppm) of glycine. The strength of the B_1 field was set to 55.5 kHz (carbon channel) and 56.8 kHz (proton channel), respectively. A total of 32 scans with a recycling delay of 2000 s were accumulated, resulting in quantitative sampling as ^{13}C spin−lattice relaxation time T_1 was found to be less than 400 s for all samples. The protons were decoupled using a TPPM (two pulse phase modulation) decoupling pulse sequence.

^1H-FIDs were acquired on a low-field Bruker spectrometer (Minispec mq20) operating at 0.5 T. The samples were cut and placed in 10 mm outer diameter NMR tubes and sealed under vacuum. It was important to limit the sample height to about 4 mm in order to obtain a reasonable rf homogeneity, and an improved magnetic-field homogeneity across the sample. Although the spectrometer provides short 90° pulses, reliable phase switching and fast digitizing, the 12 μs dead time makes reliable intensity determination of the short T_2-component difficult (T_2 of the crystalline region is of the order of 10−15 μs). Hence, all samples were later melted in order to determine the signal intensity of the FID at time t = 0. The temperature was controlled by a BVT-3000 temperature controller with temperature stability better than 1 °C. The recycle delay was initially varied in order to obtain a repetition time resulting in quantitative sampling of the FID. The observed frequency and receiver phase were adjusted manually to give a pure on-resonance absorption spectrum in order to ensure that only the real part of the FID was sampled.

Also, a Bruker DMX200 AVANCE instrument operating at 4.7 T was used which gave 90° pulse of duration 1.6 μs with a short dead time of around 3 μs. The FID was sampled every 0.2 μs with 20 s repetition time between each scan. Again, the phase parameters were adjusted to only acquire the real part of the FID. All measurements reported were performed at room temperature (23 °C), if not otherwise stated in the text.

Results and Discussion

Crystallinity Determined by ^{13}C DD-MAS. On the basis of the multiexponential behavior of the longitudinal magnetization, Horii et al.[33−35] have argued that the all-*trans*, crystalline region in the carbon NMR spectrum of PE is composed of at least three individual peaks possessing the same chemical shift. Such a multiexponential behavior of the longitudinal magnetization may be rationalized by a chain diffusion process in which chains are exchanging between the amorphous phase and the crystalline phase.[36−38] However, Veeman and co-workers[39] reported on two types of all-*trans* chains in the orthorhombic crystalline domain in all their investigated PE samples. This resulted in two clearly distinct and overlapping carbon peaks, termed n and br peaks, possessing the same chemical shift but having different line widths and different relaxation times. The claim of two separate peaks within the all-*trans* region is therefore adopted in this work.

Regarding the carbon resonance of the noncrystalline phase we realize that it must possess some degree of asymmetry since the exchange rate of a gauche−trans conformation (and hence the chemical shift) must change as the chain enters the crystalline phase. This asymmetry must therefore originate from the increasing motional constraint experienced by the part of the polymer chain which is located near the all-*trans* region. The carbon NMR spectrum of the main chain carbons has been analyzed according to a procedure analogous to that applied by Litvinov et al.[40] in which the amorphous phase is characterized by two NMR peaks. The nature of the boundary between these domains has been a subject in many investigations. For instance, the downfield peak is frequently assigned an intermediate phase.[41] Since, in this work, we are only interested in determining the crystallinity, no effort has been put into a further detailing of these individual resonance peaks.

From the above arguments the main chain carbon peaks (except for the α-carbons, β-carbons, and branch carbons) were all fitted to four distinct resonance peaks as shown in Figure 1. The nomenclature is according to De Pooter et al.[42] Importantly, many authors have adopted a pure Lorentzian line shape function in their NMR peak fitting analysis of PE. However, the actual line shape is not *a priori* known, and therefore calls for a more general type of spectral function. We found that a pseudo-Voigt function, which is a linear combination of a Lorentzian and a Gaussian

Table 1. Molar Mass ($\overline{M}_w$), Polydispersity Index ($\overline{M}_w/\overline{M}_n$), Mole Fraction Hexene (f_{hexene}), Mass Fraction Hexene (w_{hexene}), Density (ρ), and Mass Fraction Crystallinity w(DSC) Derived from DSC

copolymer	$\overline{M}_w$ (kg·mol^{-1})	$\overline{M}_w/\overline{M}_n$ [a]	f_{hexene} [b] (%)	w_{hexene} (%)	ρ (kg m^{-3})	w(DSC) (%)
A	140	2.7	0.63	1.9	928.1	55.4
B	135	2.9	0.74	2.2	933.7	59.2
C	120	3.0	1.55	4.5	928.3	56.9
D	145	2.7	1.99	5.7	921.9	52.8
E	150	3.0	2.96	8.4	918.5	50.8
F	150	3.7	3.85	10.7	915.9	49.5

[a] Determined by size exclusion chromatography (SEC) at Borealis AS. [b] Determined by high resolution ^{13}C NMR (after dissolving the polymer in ODCB at 130 °C.[30]

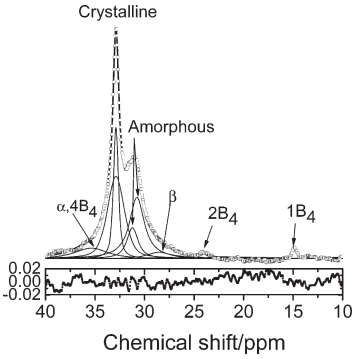

Figure 1. ^{13}C DD-MAS spectrum of sample E acquired at 23 °C. A fit to four Voigt functions (solid curve) in the main frequency domain was performed to each sample spectrum simultaneously by assuming the chemical shift and line width of each peak to be the same in each sample spectrum. The residual curve (difference between observed and calculated spectrum) is shown below the normalized spectrum (maximum signal height set to 1). The nomenclature used to assign the various peaks is according to De Pooter et al.[42]

function, to be a reasonably generalized and alternative function to use.[43]

$$I = I_0\left[m\frac{2}{\pi}\frac{\Delta}{4(\delta-\delta_c)^2+\Delta^2} + (1-m)\frac{4\ln 2}{\sqrt{\pi}\Delta}\exp\left(-\frac{\sqrt{4\ln 2}}{\Delta^2}(\delta-\delta_c)^2\right)\right] \quad (1)$$

where δ is the chemical shift, δ_c is the actual chemical shift of the resonance peak, Δ is the width at half height, m is the fraction of Lorentzian contribution to the peak ($0 \le m \le 1$) and I_0 is the peak intensity (area). The resulting model fit to eq 1 is illustrated by the solid curves in Figure 1.

The fitted spectrum in Figure 1 was obtained without any fitting constraints (except for the chemical shift of the two all-*trans* peaks which were assumed to be the same[39]). The broader peaks at $\delta = 35.5$ ppm and at $\delta = 28.6$ ppm represent the α- and β-carbons in which the $4B_4$ carbon contributes to the signal intensity of the former peak. We notice, in particular, that the signal of the chain branch carbons $1B_4$, $2B_4$, $3B_4$, and $4B_4$ were not easily detectable due to their small intensities.

It was found to be difficult to obtain reliable intensities of the two individual all-*trans* peaks, although the sum of their respective intensities was found to be reproducible. After performing the same (nonconstrained) model fit to the carbon spectrum of each sample, we noticed that each individual peak possessed—within fitting error—the same chemical shift and line width, independent of sample. This observation suggested that all six spectra could be fitted simultaneously by constraining the chemical shift and line width, i.e., by assuming the peak characteristics (chemical shift and line width) to be the same for each respective peak, independent of sample. This approach reduced the number of adjustable parameters and resulted in a more robust fitting procedure in which reproducible signal intensities of the two individual all-*trans* peaks was obtained, as well. Also, the noncrystalline region (A) was found to be characterized by a sum of two peaks, one Lorenzians and one Gaussian, possessing different chemical shifts. This asymmetry of the amorphous resonance peak (represented by the sum of two peaks with different chemical shifts) simply reflects the expected asymmetry of the spatial distribution of trans−gauche conformations within this region A. In contrast, the two all-*trans* peaks (C) are characterized by a mixture of two Gaussian/Lorenzian functions with $m_n = 0.3$ and $m_{br} = 0.6$, respectively (see eq 1). The peak characteristics of the main four peaks in the spectrum are tabulated in Table 2.

Table 2. Model-Fitted Peak Characteristics (δ, Δ and m; See Eq 1) of the Four Main Chain Carbon Peaks in the ^{13}C DD-MAS Spectra (See Figure 1), As Obtained by a Simultaneous Fit to All Spectra (See Text for Further Details)

parameter\peak	1	2	3	4
δ (ppm)	32.88	32.88	31.39	30.67
Δ (ppm)	0.411	1.141	0.998	1.343
m	0.3	0.6	0	1.0

From the above model fitting the apparent crystallinity w_{app} (eq 2) is plotted in Figure 2 against the crystallinity derived from DSC.

$$w_{app} = \frac{I_C}{I_A+I_C} = \frac{I_0(C;n)+I_0(C;br)}{I_0(A)+I_0(C;n)+I_0(C;br)} \quad (2)$$

where I_0(C;n) and I_0(C;br) are the signal intensities of the n and the br peaks within the all-*trans* region C, respectively and I_0(A) is the sum of intensities of the two noncrystalline peaks (A) in Figure 1.

The apparent crystallinity w_{app} involves neither contribution from the chain branch carbons $1B_4$, $2B_4$, $3B_4$, and $4B_4$ nor from the main chain carbons br.B_4, αB_4, and βB_4. Although these signal intensities can be estimated from the spectrum in Figure 1, their intensities are poorly defined and consequently result in rather high relative uncertainties. Hence, we found it more reliable to determine the corrected crystallinity w(C) from the known mole fraction (f) of comonomer (Table 1), according to eq 3 (see Appendix):

$$w(C) = w_{app}\frac{2-5f}{2+4f} \quad (3)$$

These corrected crystallinities are shown as black dots (●) in Figure 2 and are in excellent agreement with the crystallinities derived from DSC. Also, the mole fraction of crystallinity determined from density measurement is found to be in good agreement with DSC crystallinity (Table 1)

Finally, we will make some comments on the application of CP MAS to probe cystallinity. ^{13}C CP-MAS spectra

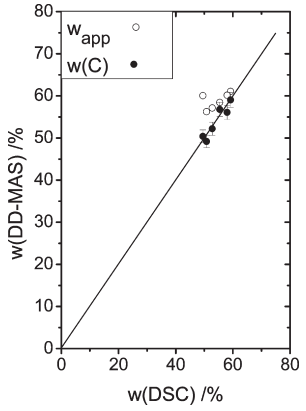

Figure 2. Apparent crystallinity w_{app} (○; eq 2) and corrected crystallinity w(C) (●; eq3), as derived from ^{13}C DD-MAS, plotted against the crystallinity determined by DSC. The solid straight line represents a one-to-one correspondence between the two crystallinities.

acquired by using eight different contact times (0.05−5 ms for each sample) were fitted simultaneously by assuming the line width and the chemical shift of each individual peak to be the same for each contact time. The resulting analysis of the signal intensity versus contact time[44] resulted in a crystallinity which was systematically larger by (5 ± 2)% compared to the crystallinity derived from ^{13}C DD-MAS. We believe this observation to be related to an insufficient enhancement of the carbon signal within the amorphous phase during CP. Work is in progress and will be reported elsewhere.

Crystallinity Determined by ^{1}H-FID NMR. *High Field (4.7 T) Proton NMR.* As pointed out in the introductory part, the crystallinity can be determined from the ^{1}H-FID if knowing the relative crystalline FID contribution to the overall FID. In the literature, we generally find two types of functions that describe this crystalline FID component. One is the Pake function:[17,45]

$$f_C^{(P)} = \sqrt{\frac{\pi}{6}} \exp\left[-\frac{1}{2}\beta^2 t^2\right] \left\{ \frac{\cos \alpha t}{\sqrt{\alpha t}} C\left[\sqrt{\frac{6\alpha t}{\pi}}\right] + \frac{\sin \alpha t}{\sqrt{\alpha t}} S\left[\sqrt{\frac{6\alpha t}{\pi}}\right] \right\} \quad (4a)$$

where $C[x]$ and $S[x]$ are the Fresnel functions, which are defined as simple integral equations[46] and the parameter α is related to the distance, R_{H-H}, between the two nearest-neighbor protons on the methylene group (eq 4b);

$$\alpha = \frac{3\gamma^2\hbar}{4R_{H-H}^3} \quad (4b)$$

where γ is the nuclear gyromagnetic ratio and $\hbar$ is Planck's constant divided by 2π. The parameter β (eq 4a) represents the width of the Gaussian broadening function, which takes account of dipole−dipole interactions between protons on different methylene groups and may be associated with the inverse of an apparent spin−spin relaxation time T_2 ($\beta = 1/T_2$). Additional details regarding the application of this function can be found in ref 17.

The second and more frequently used function to represent the crystalline part of the FID is the Abragamian function,[17,20,47−50] which takes the form:

$$f_C^{(A)} = \exp\left[-\frac{1}{2}(t/T_{2r})^2\right] \frac{\sin \omega t}{\omega t} \quad (5)$$

in which T_{2r} defines an apparent spin−spin relaxation time related to the rigid, crystalline phase and ω represents an adjustable circular frequency factor. This function was first suggested by Abragam[51] as a phenomenological expression of the ^{19}F FID of CaF_2 and is, in this work, simply denoted an "Abragamian" and has been shown to be a good representation for the FID from other, crystalline lattices. It is worth mentioning that a slightly modified version of eq 5 (in which the power coefficient 2 in eq 5 is replaced by an adjustable parameter having a value between 1 and 2) has been used by Uehara et al.[50] for characterizing highly crystalline PE samples that were etched for a long time. However, this is a rather exceptional type of function and introduces simply an additional adjustable parameter in the fit.

Concerning the FID contribution from the amorphous phase Brereton et al.[52,53] derived an exact, theoretical expression for the FID of amorphous PE above its glass transition temperature T_g. This type of function has been shown to give a satisfactory representation of the FID from PE melts over a range of temperatures. The analytical form of the "Brereton" function is rather complex and has been shown to be well approximated by a sum of a Weibullian function $W(t)$[49] and one or two exponential functions:

$$W(t) = \exp\left[-\left(\frac{t}{T_2}\right)^{\alpha}\right] \quad (6)$$

with $1 < \alpha < 2$. Hence, in this work we have used the following extended approximation of a normalized "Brereton" function to characterize the noncrystalline FID:

$$f_A = f_w \exp\left[-\left(\frac{t}{T_{2,m_1}}\right)^{\alpha 1}\right] + (1 - f_w) \exp\left[-\left(\frac{t}{T_{2,m_2}}\right)^{\alpha 2}\right] \quad (7)$$

with $1 < \alpha_1 < 2$, $0 < \alpha_2 < 1$ and $0 < f_w < 1$. The second term in eq 7 is generally known as a stretched exponential function in which $T_{2,x}$ ($x = m_1, m_2$) represents the spin−spin relaxation time of two FID-components. It needs to be emphasized that the observed FID could not be reliably fitted with a single Weibullian. The requirement of implementing a complex function such as f_A (eq 7) originates from a broad range of motional frequencies within the noncrystalline region. Also, the existence of chain branches along the main chain contributes further to this dynamic complexity. For sampling times longer than 0.2 ms the ^{1}H-FID is affected by magnetic field inhomogeneities, resulting in an apparent relaxation decay which does not necessarily reflect the true spin−spin relaxation times $T_{2,x}$.[47]

In conclusion, the normalized function used to model fit the observed ^{1}H-FID of the LLDPE samples investigated in this work takes the following form:

$$F(t) = w(H) f_C^{(X)} + (1 - w(H)) f_A \quad (8)$$

Here X equals P or A and w(H) defines the crystallinity. For simplicity we will use the short hand notation PWEs and AWEs for the two FID functions in eq 8 where P and A represent the Pake function and the Abragamian, and W and E represent the Weibullian and the stretch exponential function, respectively.

Veeman and co-workers[39] have pointed out that the protons near the crystalline br-carbons have a shorter T_2 than the protons near the crystalline n-carbons. We therefore tried to fit the observed ^{1}H-FID using two Abragamian functions. However, we were not able to obtain a reliable fit, probably due to too many adjustable parameters.

The crystallinity w(H) obtained by fitting the AWEs to the ^{1}H-FID at 4.7 T spectrometer is shown in Figure 3, and shows an excellent agreement with the crystallinity determined by ^{13}C DD-MAS NMR (and DSC).

If replacing the FID function AWEs by PWEs, the resulting goodness of the fit remained equally good. The crystallinity became systematically larger with increasing comonomer content, as reflected in Figure 3. The actual reason for the significant difference in crystallinity obtained by replacing the PWEs with the AWEs is not understood and needs further investigation. This is, however, outside the scope of this work. We simply note that the latter function results in a crystallinity which is in better agreement with the crystallinity obtained by ^{13}C DD-MAS. Also, when using the AEWs function to represent the FID, the fitting became more robust (improved reproducibility).

In the ^{13}C DD-MAS analysis we found that the spectral parameters (δ, Δ, and m) of each individual peak were the same for all samples. A corresponding constrained model fit of the ^{1}H-FID (simultaneous fit to all ^{1}H-FIDs assuming T_2, ω and α of each individual component to be the same in all FIDs, independent of sample type) suggested this to be the case also for the ^{1}H-FID. Only the relative signal intensities changed from one sample to the other. This analysis resulted in α_2 equal to 1 (exponential function) and α_1 equal to 1.35. Importantly, T_{2r} in eq 5 was found to be equal to 13.2 μs which is of the same magnitude as reported by others.[47]

As pointed out in a previous section, the main reason that the different sample FIDs possess the same NMR characteristics (T_2, ω, and α) is believed to arise from the similarities of the samples, e.g., the same thermal history, same molar mass, and same single-site catalyst, with the comonomer content being the only variable parameter.

A similar analysis of the ^{1}H-FIDs acquired at a lower magnetic field strength of 0.5 T is also depicted in Figure 3 and shows a systematically smaller crystallinity for all the samples. This will be discussed in the next section.

Low Field (0.5 T) Proton NMR. A typical ^{1}H-FID obtained at 0.5 T is illustrated in Figure 4 (sample C). In contrast to the FIDs acquired at the higher magnetic field of 4.7 T, the first point in the FIDs obtained at this lower magnetic field was acquired at 12 μs (2.8 μs at 4.7 T). The combination of short proton T_2 for the crystalline region and the long dead time (12 μs) results in a significant signal decay at the onset (t = 12 μs) of data sampling and makes it impossible to obtain a reliable crystallinity by model fitting eq 8 (using the AWEs function to represent the FID) to the observed ^{1}H-FID

In order to obtain a reliable crystallinity from such a model fit it is crucial to determine the signal intensity of the ^{1}H-FID at the shortest possible time after applying the initial rf-pulse. One way of overcoming the "dead-time" problem is to find alternative ways of estimating the signal intensity of the FID at time $t = 0$. This can best be accomplished by acquiring the ^{1}H-FID at a temperature just above the melting temperature T_m. At this temperature the signal intensity $F_{melt}(t = 12\,\mu s; T_m)$ of the FID at time $t = 12$ μs is practically equal to the signal intensity $F_{melt}(t = 0; T_m)$ of the FID at time $t = 0$, which in turn should equal the signal intensity $F_{solid}(t = 0; T_m)$ of the solid FID at time $t = 0$ and at an absolute temperature $T = T_m$. From the Curie equation, it follows that the signal intensity $F_{solid}(t = 0; T < T_m)$ of the solid FID at time $t = 0$ and at any temperature $T < T_m$ can be approximated by $F_{solid}(t = 0; T < T_m) = F_{melt}(t = 12\,\mu s; T_m)(T_m/T)$. By fitting the AWEs function to the observed ^{1}H-FID in Figure 4 and implementing the additional information about the signal intensity $F_{solid}(t = 0\ \mu s; T)$ of the FID at time $t = 0$, the crystallinity is obtained at any temperature T. Although the difference between the observed and model-fitted decay curves is rather small (<1% on an absolute scale; Figure 4, bottom), the error distribution is not random but reveals a slight oscillating behavior. It was noted that the model fit improved somewhat by adding a third Weibullian to eq 7. However, no statistical improvement was obtained.

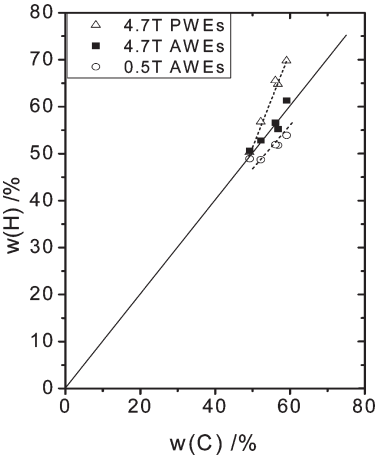

Figure 3. Crystallinity derived by ^{1}H-FID according to the two different models (PWEs, AWEs) at two different magnetic fields as a function of the crystallinity determined from ^{13}C DD-MAS spectroscopy. The solid straight line represents a one-to-one correspondence between the two crystallinities.

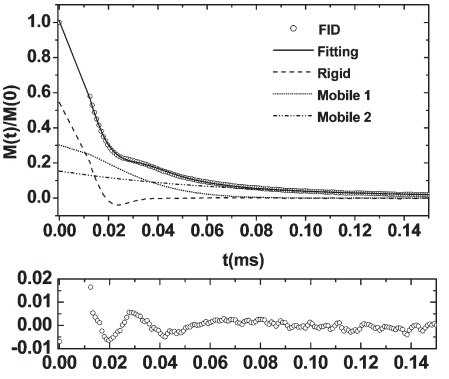

Figure 4. Top: Normalized ^{1}H-FID of sample C acquired at room temperature. The solid curve represents a nonlinear model fit to eq 8 (using the AWEs function to represent the crystalline FID component). The signal intensity at time $t = 0$ was determined from the melt. Bottom: Residual plot.

The derived crystallinity is plotted in Figure 3 and shows that all crystallinities derived at 0.5 T are systematically smaller compared to the crystallinity obtained at 4.7 T by approximately 3%, on an absolute crytallinity scale.

The reason for this discrepancy might have different origins in which the most important is believed to relate to the change in the Q-factor of the coil with temperature, which simply means that the observed FID intensity $F_{melt}(t = 12\ \mu s; T_m)$ of the melted sample must be scaled by an unknown factor k. We therefore systematically changed this factor k and remodel-fitted the FID accordingly. The results are plotted in Figure 5 and show that if multiplying the observed signal intensity by a factor $k = 1.25$, an excellent agreement between the crystallinities obtained by ^{1}H-FID analysis at the two different magnetic field strengths was obtained. A corresponding analysis of the ^{1}H-FID using the PWE function did not, however, result in reliable crystallinities. We would like to emphasize that the Factor k is simply estimated empirically

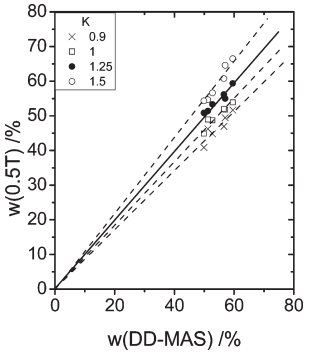

Figure 5. Crystallinity obtained from ^{1}H-FID analysis (at 0.5 T) as a function of the crystallinity derived from ^{13}C DD-MAS spectra. The parameter k represents a calibration factor which takes into account a change in the Q-factor of the coil after heating the solid polymer to a temperature above its melting point. The best fit is obtained for $k = 1.25$ (see text for further details).

Conclusion

^{13}C DD-MAS NMR spectra of semicrystalline ethene-1-hexene copolymers were shown to be excellently model fitted to four pseudo Voigt functions (linear combination of Gaussian and Lorentzian functions). In order to mimic the asymmetric properties of the amorphous phase, it was fitted to a sum of two pseudo Voigt functions possessing different chemical shifts. The two other resonance peaks, having the same chemical shift but differing in line width, were assigned to the all-*trans* crystalline domain. By correcting for the lack of discernible side-chain resonances, the derived crystallinity was found to be in excellent agreement with the crystallinity derived from DSC.

The corresponding crystallinity obtained from ^{1}H-FID acquired at 4.7 T (dead time of approximately 3 μs) was found to be consistent with the crystallinity obtained by ^{13}C DD-MAS NMR.

In contrast, the crystallinity derived from the ^{1}H-FID acquired at 0.5 T revealed a systematically smaller value by approximately 3% on an absolute crytallinity scale, and is explained by a significant blanking of the initial part of the FID due to a rather long dead time (on the order of 12 μs). In order to partially compensate for this dead-time effect, the signal intensity of the FID at time zero was set equal to the corresponding FID intensity of the melted sample (after correcting the latter intensity by the well-known Curie law). However, compared to the crystallinity derived from the ^{1}H-FID at 4.7 T, the crystallinity determined from the 1H-FID at 0.5 T still remained somewhat samller, and was rationalized by a change in the Q-factor of the coil with temperature. Hence, after multiplying the observed FID intensity (at $t = 0$) of the melt by a factor of 1.25 before model-fitting, an excellent agreement between the crystallinities derived from the ^{1}H-FID analysis at the two different magnetic field strengths was obtained.

Finally, we want to point out that after replacing the Abragamian function by a Pake function to represent the crystalline part of the FID, a poorer reproducibility in the derived crystallinity was noted, probably because of numerical instabilities.

Acknowledgment. The authors would like to thank the Norwegian Research Council (NFR) for financial support. Also, L.Z. wants to thank professor Q. Chen (East China Normal University, Shanghai) and Professor K. Saalwächter (Martin-Luther-Universität Halle-Wittenberg) for many illuminating discussions and, in particular, for placing their NMR laboratory facilities at her disposal. Also, we would like to thank the referees for interesting comments and suggestions.

Appendix

If we define the apparent crystallinity w_{app} by the number of carbons ($2N_E^{(C)}$) within the all-*trans* domain divided by the total number of observable main chain carbons ($2N_E^0 - 3N_H^0$) we may write:

$$w_{app} = \frac{2N_E^{(C)}}{2N_E^0 - 3N_H^0} \quad \text{(A1)}$$

where $N_H^{(0)}$ represents the number of C_4 branches (which equals the number of hexene molecules). In eq A1 we have excluded signal intensity of the α-carbons, the β-carbons, and the br-carbon but included the intensity from the $4B_4$-carbon, which is located within the noncrystalline region of the spectrum, hence the term ($-3N_H^0$). The actual crystallinity is defined by eq A2

$$w(C) = \frac{2N_E^{(C)}}{2N_E^0 + 6N_H^0} \quad \text{(A2)}$$

where the mole fraction f of comonomer (hexene) is defined by:

$$f = \frac{N_H^0}{N_H^0 + N_E^0} \quad \text{(A3)}$$

By combining eq A1−A3, we obtain eq 3 in the main text.

References and Notes

(1) Mandelkern, L.; Peacock, A. J. *Stud. Phys. Theor. Chem.* **1988**, *54*, 201–227.
(2) Popli, R.; Mandelkern, L. *J. Polym. Sci., Part B: Polym. Phys.* **1987**, *25*, 441–483.
(3) Obande, O. P.; Gilbert, M. *J. Appl. Polym. Sci.* **1989**, *37*, 1713–1726.
(4) Kavesh, S.; Schultz, J. M. *Polym. Eng. Sci.* **1969**, *9*, 331–338.
(5) Moore, W. H.; Krimm, S. *Makromol. Chem.* **1975**, Suppl. 1, 491−506.
(6) Guerrero, S. J.; Veloso, H.; Randon, E. *Polymer* **1990**, *31*, 1615–1622.
(7) Illers, K. H. *J. Macromol. Sci., Phys.* **1977**, *B14*, 471–482.
(8) Asano, A.; Tanaka, C.; Murata, Y. *Polymer* **2007**, *48*, 3809–3816.
(9) Barendswaard, W.; Litvinov, V. M.; Souren, F.; Scherrenberg, R. L.; Gondard, C.; Colemonts, C. *Macromolecules* **1999**, *32*, 167–180.
(10) Thakur, K. A. M.; Kean, R. T.; Zupfer, J. M.; Buehler, N. U.; Doscotch, M. A.; Munson, E. J. *Macromolecules* **1996**, *29*, 8844–8851.
(11) Maus, A.; Hertlein, C.; Saalwaechter, K. *Macromol. Chem. Phys.* **2006**, *207*, 1150–1158.
(12) Bridges, B. J.; Charlesby, A.; Folland, R. *Proc. R. Soc. London, Ser. A* **1979**, *367*, 343–351.
(13) Feio, G.; Buntinx, G.; Cohen-Addad, J. P. *J. Polym. Sci., Part B: Polym. Phys.* **1989**, *27*, 1–24.
(14) Feio, G.; Cohen-Addad, J. P. *J. Polym. Sci., Part B: Polym. Phys.* **1988**, *26*, 389–412.
(15) Ebengou, R. H.; Cohen-Addad, J. P. *Polymer* **1994**, *35*, 2962–2969.
(16) Zhang, S.; Wu, X.; Mehring, M. *Chem. Phys. Let.* **1990**, *173*, 481–484.
(17) Hansen, E. W.; Kristiansen, P. E.; Pedersen, B. *J. Phys. Chem. B* **1998**, *102*, 5444–5450.
(18) Kristiansen, P. E.; Hansen, E. W.; Pedersen, B. *J. Phys. Chem. B* **1999**, *103*, 3552–3558.
(19) Kristiansen, P. E.; Hansen, E. W.; Pedersen, B. *Polymer* **2000**, *42*, 1969–1980.
(20) Litvinov, V. M.; Penning, J. P. *Macromol. Chem. Phys.* **2004**, *205*, 1721–1734.
(21) Zhang, S.; Wu, X. *Chem. Phys. Lett.* **1989**, *156*, 82–86.
(22) Rhim, W. K.; Pines, A.; Waugh, J. S. *Phys. Rev. B* **1971**, *3*, 684–696.
(23) Matsui, S. *Chem. Phys. Lett.* **1991**, *179*, 187–190.
(24) Yamanobe, T., *Solid State NMR of Polymers*; Elsevier: Amsterdam, 1998.
(25) VanderHart, D. L.; Asano, A.; Gilman, J. W. *Chem. Mater.* **2001**, *13*, 3796–3809.
(26) Hu, W. G.; Schmidt-Rohr, K. *Polymer* **2000**, *41*, 2979–2987.
(27) Young, S. G.; Magill, J. H. *Macromolecules* **1989**, *22*, 2549–2551.
(28) Zhang, L.; Liu, Z.; Chen, Q.; Hansen, E. W. *Macromolecules* **2007**, *40*, 5411–5419.
(29) Glowinkowski, S.; Makrocka-Rydzyk, M.; Wanke, S.; Jurga, S. *Eur. Polym. J.* **2002**, *38*, 961–969.

(30) Hansen, E. W.; Blom, R.; Bade, O. M. *Polymer* **1997**, *38*, 4295–4304.
(31) Mathot, V. B. F.; Pijpers, M. F. J. *J. Therm. Anal.* **1983**, *28*, 349–358.
(32) ATHAS, http://athas.prz.rzeszow.pl/.
(33) Kuwabara, K.; Kaji, H.; Horii, F. *Macromolecules* **2000**, *33*, 4453–4462.
(34) Kuwabara, K.; Kaji, H.; Tsuji, M.; Horii, F. *Macromolecules* **2000**, *33*, 7093–7100.
(35) Chaiyut, N.; Amornsakchai, T.; Kaji, H.; Horii, F. *Polymer* **2006**, *47*, 2470–2481.
(36) Klein, P. G.; Driver, M. A. N. *Macromolecules* **2002**, *35*, 6598–6612.
(37) Robertson, M. B.; Ward, I. M.; Klein, P. G.; Packer, K. J. *Macromolecules* **1997**, *30*, 6893–6898.
(38) Klein, P. G.; Robertson, M. B.; Driver, M. A. N.; Ward, I. M.; Packer, K. J. *Polym. Int.* **1998**, *47*, 76–83.
(39) Hillebrand, L.; Schmidt, A.; Bolz, A.; Hess, M.; Veeman, W.; Meier, R. J.; van der Velden, G. *Macromolecules* **1998**, *31*, 5010–5021.
(40) Litvinov, V. M.; Mathot, B. F. *Solid State Nucl. Magn. Reson.* **2002**, *22*, 218–234.
(41) Kitamaru, R.; Horii, F.; Murayama, K. *Macromolecules* **1986**, *19*, 636–643.
(42) De Pooter, M.; Smith, P. B.; Dohrer, K. K.; Bennett, K. F.; Meadows, M. D.; Smith, C. G.; Schouwenaars, H. P.; Geerards, R. A. *J. Appl. Polym. Sci.* **1991**, *42*, 399–408.
(43) Wertheim, G. K.; Butler, M. A.; West, K. W.; Buchanan, D. N. E. *Rev. Sci. Instrum.* **1974**, *45*, 1369–1371.
(44) Kolodziejski, W.; Klinowski, J. *Chem. Rev.* **2002**, *102*, 613–628.
(45) Look, D. C.; Lowe, I. J.; Northby, J. A. *J. Chem. Phys.* **1966**, *44*, 3441–3452.
(46) Abramowitz, M.; Stegun, I. A., *Handbook of mathematical functions with formulas, graphs, and mathematical table*; Courier Dover Publications: 1965, p300.
(47) Hedesiu, C.; Demco, D. E.; Kleppinger, R.; Buda, A. A.; Blümich, B.; Remerie, K.; Litvinov, V. M. *Polymer* **2007**, *48*, 763–777.
(48) Litvinov, V. M. *Macromolecules* **2006**, *39*, 8727–8741.
(49) Dadayli, D.; Harris, R. K.; Kenwright, A. M.; Say, B. J.; Sunnetcioglu, M. *Polymer* **1994**, *35*, 4083–4087.
(50) Uehara, H.; Aoike, T.; Yamanobe, T.; Komoto, T. *Macromolecules* **2002**, *35*, 2640–2647.
(51) Abragam, A., *The Principles of Nuclear Magnetism.* Oxford University Press: Oxford, U.K., 1961.
(52) Brereton, M. G. *J. Chem. Phys.* **1991**, *94*, 2136.
(53) Brereton, M. G.; Ward, I. M.; Boden, N.; Wright, P. *Macromolecules* **1991**, *24*, 2068–2074.